Structural Amorphous Steels

Z. P. Lu,[1,*] C. T. Liu,[1] J. R. Thompson,[2,3] and W. D. Porter[1]

[1]*Metals and Ceramics Division, Oak Ridge National Laboratory, Oak Ridge, Tennessee 37831-6115, USA*
[2]*Condensed Matter Science Division, Oak Ridge National Laboratory, Oak Ridge, Tennessee 37831-6061, USA*
[3]*Department of Physics, University of Tennessee, Knoxville, Tennessee 37996-1200, USA*

(Received 19 March 2004; published 16 June 2004; corrected 19 July 2004)

Recent advancement in bulk metallic glasses, whose properties are usually superior to their crystalline counterparts, has stimulated great interest in fabricating bulk amorphous steels. While a great deal of effort has been devoted to this field, the fabrication of structural amorphous steels with large cross sections has remained an alchemist's dream because of the limited glass-forming ability (GFA) of these materials. Here we report the discovery of structural amorphous steels that can be cast into glasses with large cross-section sizes using conventional drop-casting methods. These new steels showed interesting physical, magnetic, and mechanical properties, along with high thermal stability. The underlying mechanisms for the superior GFA of these materials are discussed.

DOI: 10.1103/PhysRevLett.92.245503 PACS numbers: 81.05.Kf, 61.43.Dq, 62.20.–x, 75.20.En

Although conventional steels with crystalline structures have been extensively utilized by industries, bulk amorphous steels (BASs) show great potential to supersede these crystalline steels for some critical structural and functional applications because of their unusual combinations of engineering properties: these include higher strength and hardness, better magnetic properties, and better corrosion resistance [1–6]. Moreover, compared with most other bulk amorphous alloy systems such as Zr- and Pd-based bulk metallic glasses, BASs offer some important advantages: much lower material cost, higher strength, better magnetic properties, better corrosion resistance, and higher thermal stability (the glass transition temperatures are close to or above 900 K) [3,7,8]. However, a major obstacle to the feasibility of Fe-based amorphous steels is their limited glass-forming ability (GFA). The BASs with the best GFA reported so far can be cast only into a rod with a diameter of $\sim$4 mm by injecting the molten alloy into a copper mold [3]. Hence, it is necessary to improve the GFA of Fe-based alloys in order to enhance their ability to form bulk glassy steels under conventional industrial conditions, using, for example, commercial-grade raw materials, low vacuum furnace, conventional casting methods, etc. Thus, such steels could be more viable for engineering applications.

In this study, the best BAS reported recently [3] was chosen as a starting composition because of its known thermal properties and GFA. Alloy ingots were obtained by arc-melting a mixture of commercial-grade metals (with purities from 99% to 99.9%), boron crystal, carbon rod, and the master alloy Fe-33%Y in a purified argon atmosphere. The resultant homogeneous alloys were then remelted in a Zr-gettered argon atmosphere on the top of a copper mold with various diameters, and the molten liquids were thus drop-cast into a copper mold using their own gravity.

The amorphous nature was ascertained by x-ray diffraction (XRD) and optical microscopy. The thermal properties associated with the glass transition, supercooled liquid, and crystallization of the newly developed glassy steels were examined by a Netzsch model 404 DSC (differential scanning calorimetry) at a heating rate of 20 K/min in a flow of purified argon gas after evacuating to $\sim 10^{-3}$ torr. The melting and solidification behavior of these steels were also investigated by continuous DSC heating and cooling measurements at the same rate of 20 K/min, respectively. The samples for melting and solidification studies were annealed at 900 °C for 24 h under high vacuum prior to the DSC measurements. A MHT hardness tester was employed to determine the Vickers hardness of these steels under a load of 300 g. Compression tests were carried out using a MTS hydraulic testing system with a strain rate of 10^{-3} s^{-1}. The density of the glassy steels was measured using an Accupyc^{TM} 1330 pycnometer. The magnetic response of the BASs was investigated over the temperature range 5–400 K using two SQUID-based magnetometers. Nanoindentation experiments were conducted at 23 °C using a Nanoindenter® XP (Nano Instruments Innovation Center, MTS Corporation, Knoxville, TN). A Berkovich diamond indenter (three-sided pyramidal tip) was used and the experiments were run in load control at a constant $\dot{P}/P$ rate ($= 0.05$ s^{-1}) to a prescribed maximum load that ranged from 3 to 20 mN.

Figure 1 is a pseudoternary phase diagram showing nominal compositions of new glassy steels with a fixed yttrium content of 1.5% (all compositions herein are in atomic percent). As can be seen, glassy steels with a diameter of at least 12 mm can be prepared for the compositions inside the small box, while 7-mm rods with fully amorphous structures can be obtained in a relatively large composition range. The boundaries of the boxes indicate the composition limits of metal elements (i.e., Mo + Mn) and metalloids (i.e., B + C) for bulk glass formation, respectively. The preferable glass-forming composition is approximately formulated as

 © 2004 The American Physical Society

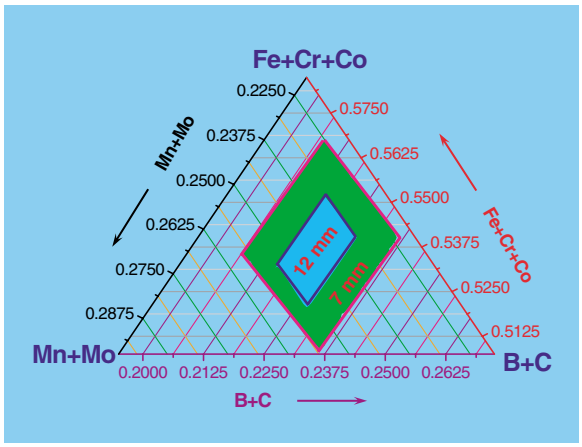

FIG. 1 (color online). A pseudoternary phase diagram showing the glass-forming compositions with fixed yttrium content of 1.5%. The numbers inside the diagram indicate the attained diameters of glassy rods prepared by a conventional copper casting technique.

$(Fe_{67.1-a-b-c}Cr_aCo_bMo_cMn_{11.2}C_{150.8}B_{5.9})_{98.5}Y_{1.5}$, wherein $4 \leq a \leq 10$; $b \leq 6$; and $12.5 \leq c \leq 14$.

Figure 2 shows XRD patterns for as-cast samples of two representative glassy steels. Here the compositions are $(Fe_{44.3}Cr_5Co_5Mo_{12.8}Mn_{11.2}C_{15.8}B_{5.9})_{98.5}Y_{1.5}$ (denoted as steel *B*) and $(Fe_{44.3}Cr_{10}Mo_{13.8}Mn_{11.2}C_{15.8}B_{5.9})_{98.5}Y_{1.5}$ (steel *C*). For comparison, the XRD pattern for an as-cast, 7-mm sample of a steel with no yttrium [i.e., $Fe_{44.3}Cr_5Co_5Mo_{12.8}Mn_{11.2}C_{15.8}B_{5.9}$ (steel *A*)] is also included. For both steels *B* and *C* with as-cast diameters up to 12 mm, the XRD traces reveal only two typical halos, and no peaks corresponding to crystalline phases are visible. These features indicate that these samples consist of a mostly amorphous structure, and fully glassy materials up to 12 mm in diameter can be formed in both compositions. In contrast, steel *A* (7 mm diameter, as-cast) containing no yttrium exhibits crystalline peaks superimposed on the main halo peaks, suggesting that the GFA of this steel is much lower than that of steels *B* and *C*.

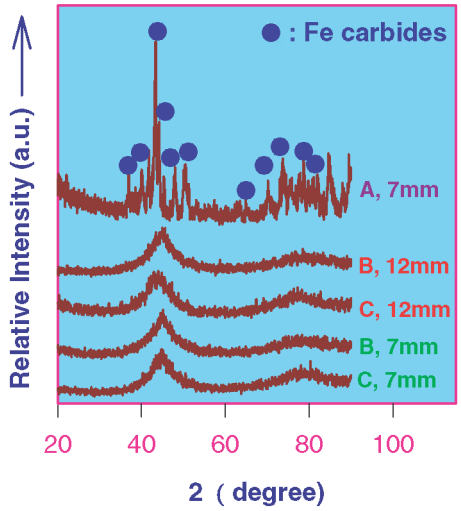

FIG. 2 (color online). XRD patterns of three glass-forming steels showing the amorphous nature of drop-cast samples *B* and *C* and the striking effect of yttrium on glass formation. *A*: $Fe_{44.3}Cr_5Co_5Mo_{12.8}Mn_{11.2}C_{15.8}B_{5.9}$ with no yttrium, *B*: $(Fe_{44.3}Cr_5Co_5Mo_{12.8}Mn_{11.2}C_{15.8}B_{5.9})_{98.5}Y_{1.5}$, and *C*: $(Fe_{44.3}Cr_{10}Mo_{13.8}Mn_{11.2}C_{15.8}B_{5.9})_{98.5}Y_{1.5}$.

The thermal properties of glassy steels *B* and *C* obtained by DSC are shown in Fig. 3. These DSC scans clearly exhibit the glass transition and crystallization events, indicating that these steels have a mostly amorphous structure. The density, microhardness, and the glass transition temperature T_g of 12-mm, drop-cast samples of steels *B* and *C* are tabulated in Table I. Mechanical properties of these novel glassy steels were also measured at the length scale of shear bands through the use of nanoindentation. Figure 4 shows a typical load-displacement (P-h) curve for steel *B* with a loading rate $(\dot{P}/P)$ of 0.05 s^{-1}. The inset is the image of deformation around an ultrafine-scale Berkovich indent, clearly exhibiting slip band markings as a result of localized plastic flow. The averaged hardness and Young's modulus determined from the nanoindentation measurements are also given in Table I, together with the ultimate strength from the compression tests. The density of these glassy steels is around 7.8 g/cm^3, lower than that of ultrahigh strength maraging steels (i.e., ~8.1 g/cm^3) [9]. However, current glassy steels are much stronger; their hardness values are more than twice that of the maraging steels [9]. In addition, the present BASs are also stronger than other types of bulk metallic glasses. For example, the Young's modulus and average hardness obtained from the nanoindentation for bulk $Pd_{40}Cu_{30}Ni_{10}P_{20}$ metallic glass are 105 and

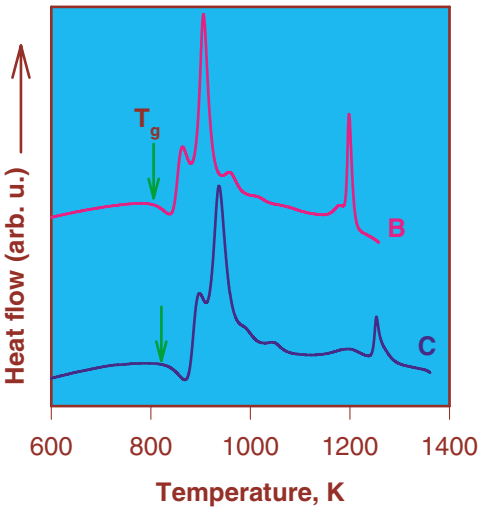

FIG. 3 (color online). DSC scans of as-cast, 12 mm glassy steels *B* and *C*.

TABLE I. Thermal properties and mechanical properties for two representative bulk amorphous steels.

Steel no.	Maximum size (mm)	T_g (K)	T_m (K)	T_l (K)	Density (g/cm^3)	Vickers hardness (HV)	Compression strength (MPa)	Young's modulus (GPa)	Nanoindentation hardness (GPa)
A	<7	···	1341.2	1491.5	···	···	···	···	···
B	≥ 12	804.0	1344.3	1411.4	7.89	1224 ± 50	~3000	257.1 ± 16.6	14.8 ± 1.2
C	≥ 12	835.5	1368.9	1439.8	7.83	1287 ± 45	···	···	···

4.75 GPa, respectively [10]. As shown in Table I, the Young's modulus of the new glassy steels is more than double, while the nanoindentation hardness values are almost triple, that of bulk $Pd_{40}Cu_{30}Ni_{10}P_{20}$ metallic glass. In addition, all the new BASs are paramagnetic at room temperature and become ferromagnetic at cryogenic temperatures. The magnetization $M(H)$ of steel *B* at various temperatures, together with the magnetic susceptibility in low fields, indicate that the Curie temperature T_c of this alloy lies near 55 K [11]. Nonferromagnetic behavior at ambient temperatures will open up new industrial and engineering applications for these steels.

To understand the underlying mechanisms of why the current glassy steels have superior GFA, the melting and solidification behavior of steel *B* have been studied by continuous heating and cooling DSC experiments, respectively, as shown in Fig. 5. For comparison, the corresponding results for steel *A* are included as well. The onset melting temperature T_m and offset melting temperature T_l (apparent liquidus temperature) of these three steels are also listed in Table I. During cooling, as shown in Fig. 5, two major exothermic peaks are observed for the steel without the addition of yttrium (i.e., steel *A*). The first, small peak (circled) is due to the formation of Fe carbides (see the XRD results in Fig. 2) while the large peak is ascribed to the solidification of the eutectic. The cooling curve of steel *B* is essentially a single peak, and the small, high-temperature peak corresponding to the formation of Fe carbides in steel *A* is completely suppressed. All of these indicate that steel *B* is very close to the eutectic and steel *A* has an off-eutectic composition. During heating, steel *A* displays a wide endothermic peak at an onset temperature of 1341.2 K, followed by a small peak at the high temperature (also circled), which is due to the melting of Fe carbides. This observation is consistent with the continuous DSC cooling results of this steel and further confirmed that steel *A* is off-eutectic with a eutectic reaction likely at 1341.2 K. On the other hand, the heating DSC curve of steel *B* shows only a single peak associated with the melting of the eutectic at an onset temperature of 1341.3, and the peak due to the melting of Fe carbides (as in the case of steel *A*) is not visible. Consequently, the liquidus temperature (T_l) is decreased significantly from 1491.5 K for steel *A* to 1411.4 K for steel *B*. Both steels seem to have the same eutectic event occurring near 1341 K. The irregular shape of the melting

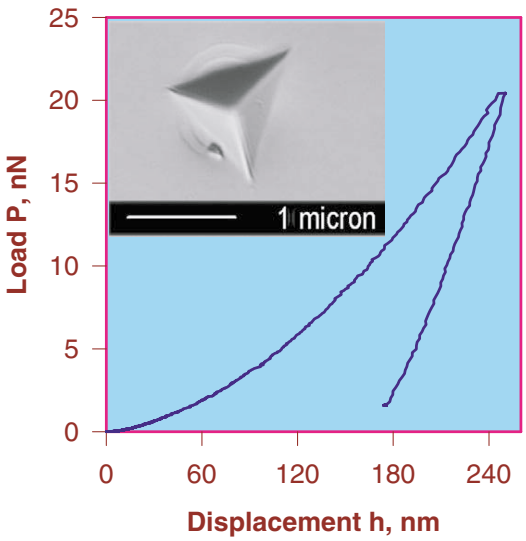

FIG. 4 (color online). Typical load-displacement (*P-h*) loading and unloading curves measured by nanoindentation experiments. The inset exhibits localized plastic flow aroused from the shear bands activation around a Berkovich indent.

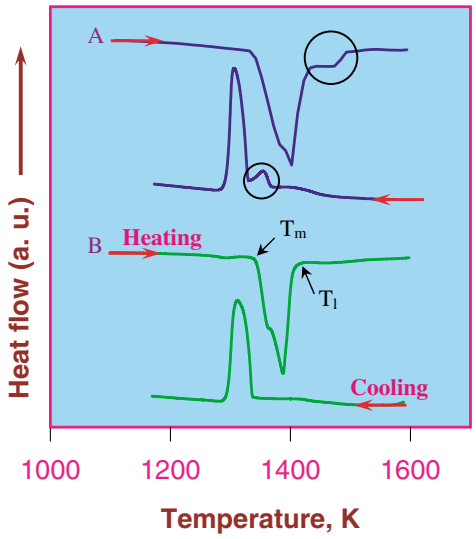

FIG. 5 (color online). The DSC cooling and heating curves for glassy steels *A* and *B* obtained at a scanning rate of 20 K/min. Circled peaks on DSC cooling and heating curves of steel *A* are due to the formation and melting of Fe carbides, respectively. The samples were equilibrated at 900 °C for 24 h under high vacuum.

peak of these multicomponent steels suggests that the "deep" eutectics are likely composed of various low-order eutectics such as binary and ternary eutectics with close melting points. This phenomenon was also reported even in a ternary bulk Zr-Cu-Al system [12].

Therefore, the underlying mechanisms of the superior GFA of the novel bulk glassy steels can be twofold; first, the compositions of the present BASs are associated with deep eutectics of the current Fe-(C, B) system. The eutectic temperatures (i.e., the onset melting points T_m) of these steels are more than 80–100 K lower than those of the best glass-forming compositions in a similar system reported so far [13], suggesting that these new steels are at or close to the deep eutectic. It is well known that compositions around the deep eutectic are the best compositions for glass formation in any given system. At such points, the liquids have the largest stability and ordering [14,15]. As a result, glass formation is greatly favored thermodynamically. Second, the minor addition of yttrium strikingly promotes glass formation in the Fe-(C, B) system via suppressing the formation of the primary phase. Without the addition of yttrium, for example, steel A cannot form glass in a sample with a diameter of 7 mm, while steel B with 1.5% Y can be cast into a 12 mm diameter rod with fully amorphous structure (see Fig. 1; note that detailed optimization of yttrium contents will be published elsewhere [11]). Because of their limited solubility in the Fe carbides, the yttrium atoms must redistribute and long-range diffusion is required upon solidification. Thus, the minor addition of yttrium can effectively retard the nucleation and growth of the primary phase (i.e., Fe carbides) upon cooling, leading to a dramatic depression in the liquidus temperature (T_l). In other words, the yttrium addition in steel A not only destabilizes the competing crystalline phases but also stabilizes the liquid phases. As a consequence, glass formation in steel B is favored both kinetically and thermodynamically, resulting in an evident enhancement of the GFA [16]. The addition of yttrium effectively shifts the steel composition from off-eutectic to the eutectic.

In summary, a series of novel structural glassy steels have been successfully synthesized. The superior GFA of these BASs enables a successful preparation of large structural components using commercial melting and casting techniques. These BASs exhibit a unique combination of physical, mechanical, and magnetic properties, along with high thermal stability. The striking enhancement of the GFA in these new steels is attributed to two factors: (1) their compositions are associated with deep eutectics, and (2) the minor addition of yttrium adjusts their compositions close to the eutectic points. The current work demonstrates that a minor alloying technique is extremely effective in promoting bulk glass formation.

This research was sponsored by the Division of Materials Sciences and Engineering, Office of Basic Energy Sciences, and by the Assistant Secretary for Energy Efficiency and Renewable Energy, Office of Freedom CAR and Vehicle Technology Program, as part of the High Temperature Materials Laboratory User program. Oak Ridge National Laboratory (ORNL) is managed by UT-Battelle LLC, for U.S. Department of Energy under Contract No. DE-AC05-00OR-22725. The authors are also grateful to Dr. H. Bei for his help in nanoindentation experiments.

Note added.—After submitting our manuscript, we found that independent research conducted by Ponnambalam *et al.* [17] also indicates that minor alloy additions of rare-earth elements have significantly beneficial effects on glass formation in Fe-based alloys.

*Corresponding author.
Electronic address: luzp@ornl.gov

[1] W. L. Johnson, JOM **54**, 40 (2002).
[2] A. Inoue, in *Bulk Amorphous Alloys: Practical Characteristics and Applications* (Trans Tech Publications Ltd., Switzerland, 1999).
[3] V. Ponnambalam *et al.*, Appl. Phys. Lett. **83**, 1131 (2003).
[4] A. Inoue and X. M. Wang, Acta Mater. **48**, 1383 (2000).
[5] S. J. Pang, T. Zhang, K. Asami, and A. Inoue, Acta Mater. **50**, 489 (2002).
[6] T. D. Shen and R. B. Schwarz, Appl. Phys. Lett. **75**, 49 (1999).
[7] Z. P. Lu, C. T. Liu, C. A. Carmichael, W. D. Porter, and S. C. Deevi, J. Mater. Res. **19**, 921 (2004).
[8] A. Inoue, T. Zhang, and A. Takeuchi, Appl. Phys. Lett. **71**, 464 (1997).
[9] http://asm.matweb.com/search/SpecificMaterial.asp?bassnum=NALL77 and http://www.matweb.com/search/GetProperty.asp.
[10] Yu. I. Golovin *et al.*, Scr. Mater. **45**, 947 (2001).
[11] Z. P. Lu, C. T. Liu, and W. D. Porter (unpublished).
[12] Y. Yokoyama, H. Inoue, K. Fukaura, and A. Inoue, Mater. Trans., JIM **43**, 575 (2002).
[13] Z. P. Lu, C. T. Liu, and W. D. Porter, Appl. Phys. Lett. **83**, 2581 (2003).
[14] M. H. Cohen and D. Turnbull, Nature (London) **189**, 131 (1961).
[15] R. J. Highmore and A. L. Greer, Nature (London) **339**, 363 (1989).
[16] Z. P. Lu and C. T. Liu, Phys. Rev. Lett. **91**, 115505 (2003).
[17] V. Ponnambalam *et al.*, J. Mater. Res. **19**, 1320 (2004).